

# Deuteron Electrodisintegration at Threshold at Large Momentum Transfers

J. Jourdan\*, D. Rohe, I. Sick, G.A. Warren\*  
*University of Basel, Basel, Switzerland*

J.M. Finn  
*College of William and Mary, Williamsburg, VA*

W. Boeglin  
*Florida International University, Miami, FL*

J. Templon  
*University of Georgia, Athens, GA*

J.J. LeRose, J. Mitchell, A. Saha  
*Jefferson Lab, Newport News, VA*

P. Ulmer  
*Old Dominion University, Norfolk, VA*

S.E. Rock  
*Stanford Linear Accelerator Center, Menlo Park, CA*

D. Crabb, D.B. Day, R.C. Minehart, O. Rondon Aramayo,  
F. Wesselmann, H. Zhu  
*University of Virginia, Charlottesville, VA*

\* Spokepersons

## Abstract

We propose a single arm  $d(e,e')$  threshold electrodisintegration experiment at electron energies up to 1.6 GeV in Hall A. The isovector magnetic dipole transition from the ground state to the nearly bound  $^1S_0$  state dominates the cross section at threshold so that the process is sensitive to meson exchange currents in the nucleon-nucleon interaction. This experiment will extend the data up to the highest possible momentum transfer, limited by a cross section of  $9 \cdot 10^{-42} \text{ cm}^2/\text{sr MeV}$ , as well as significantly improve on the uncertainties of the existing data. In the available region of momentum transfer, it is expected that the hadron-based picture of the nucleon-nucleon interaction begins to break down and quark and gluon degrees of freedom become important.

The excitation energy resolution will be 1.5 MeV, providing a separation from the elastic process, as well as allowing a measurement of the  $E_{np}$  dependence of the cross section. We request a total beam time of 20 days and an additional 4 days for setup and decommissioning.

# 1 Introduction

One of the fundamental goals of nuclear physics is to understand how the nucleus is constructed. This construction, in the non-relativistic limit, is dominated by the interaction between two nucleons. The deuteron, the only stable two nucleon system, is the ideal place to test our understanding.

An electromagnetic probe of the deuteron interacts with several currents in the 2N system. There are the nucleonic currents which are related to the wavefunction of the nucleon in the nucleus. There are the isobar configuration (IC) currents which are related to the excited states of the nucleon in the nucleus. And there are meson exchange currents (MEC) which, as the name implies, are sensitive to the mesons exchanged between the two nucleons. As the long and medium range NN interaction is described by meson exchange, measurements of the MEC are crucial for our understanding of the NN system.

Deuteron electrodisintegration at threshold provides a textbook example of such a measurement. The transition from the  ${}^3S_1 + {}^3D_1$  ground state to the barely unbound  ${}^1S_0$  first excited state is an isovector (IV) magnetic dipole (M1) transition. MEC are enhanced relative to the nucleonic currents in this type of transition. By performing the measurement at backward angles where the longitudinal and elastic contributions are small, sensitivity to the IV M1 transition is enhanced. The transition reveals itself as a cusp in the cross section just above the disintegration threshold, see Fig. 1 for an example.

In the earliest low  $Q^2$  measurements, deuteron electrodisintegration at threshold revealed its strength in measuring non-nucleonic degrees of freedom in the NN interaction. The results of the first part of these experiments, which were performed at Saclay [1] and reached up to  $Q^2 \leq 10 \text{ fm}^{-2}$ , disagreed with the initial impulse approximation (IA) model calculations which included only the  ${}^3S_1$  and  ${}^3D_1$  components of the deuteron ground state, see Fig. 2. The calculation predicted a deep minimum at  $Q^2 \approx 12 \text{ fm}^{-2}$  due to an interference between the  ${}^3S_1 \rightarrow {}^1S_0$  and the  ${}^3D_1 \rightarrow {}^1S_0$  transitions. After pion exchange currents ( $\pi$ EC) and IC were

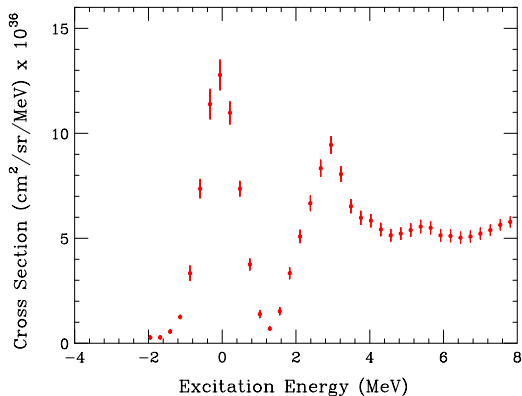


Figure 1: Distribution of scattered electrons from deuterium at  $155^\circ$  with a beam energy of 360 MeV. The elastic peak is at zero excitation energy and the cusp due to the  ${}^1S_0$  state is at  $\approx 3$  MeV. Taken from Ref. [1].

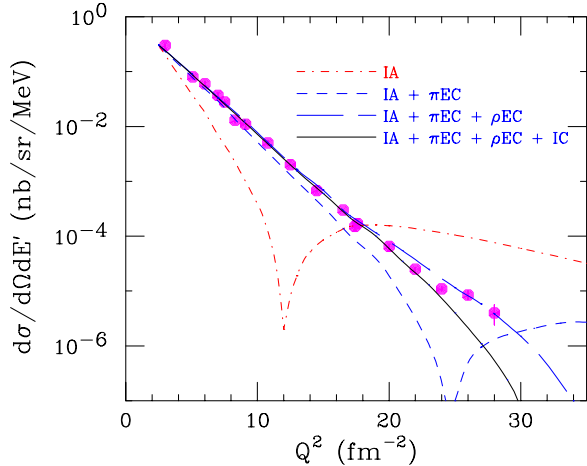


Figure 2: Early data from Saclay and calculation of Mathiot [2] with contributions from different mechanisms.

included, the data and theory agreed [2], but the IA+ $\pi$ EC calculation predicted a minimum at  $Q^2 \approx 28 \text{ fm}^{-2}$ . Additional data up to  $Q^2 = 28 \text{ fm}^{-2}$ , however, showed a smooth fall-off without an interference minimum. The addition of heavier meson exchange, up to  $\rho$  exchange, become necessary to describe the data.

Models of the NN interactions in terms of hadron degrees of freedom provide a reasonable description of the 2N system, including MEC and IC, in the non-relativistic limit [3, 5, 4, 6]. At a high momentum transfer, where the wavefunctions of the two nucleons significantly overlap, we expect quark and gluon degrees of freedom to become important. In fact, as one approaches high momentum transfer, the concept of nucleonic constituents and exchange mesons is blurred and eventually lost altogether as one begins to describes the deuteron as composed of valence quarks, a sea and glue. Deuteron electrodisintegration at threshold, because it is sensitive to non-nucleonic contributions, is a good place to look for this transition from hadron to quark-gluon degrees of freedom.

Deuteron electrodisintegration at threshold experiments have always been high profile experiments because of the physics one can learn from them. The PAC14 Few-Body Workshop in 1998 reviewed the few-body program at JLab and outlined the questions which motivated the program [7]. The two experimental questions were:

- Can few-body systems be understood in terms of a “*standard model*” for nuclear physics with only nucleon degrees of freedom?
- Are quark/gluon degrees of freedom required in understanding selected properties of the few-body system?

Deuteron electrodisintegration at threshold was the first of the listed possible experiments to address these questions, perhaps, because it can provide some of the cleanest information to address both of these questions.

The experiment presented in this proposal will significantly improve on previous measurements. It will dramatically extend the range of  $Q^2$  for high resolution experiments, from  $42 \text{ fm}^{-2}$  to  $95 \text{ fm}^{-2}$ , in search of evidence of the quark-gluon degrees of freedom. Low resolution data exist up to  $Q^2 = 70 \text{ fm}^{-2}$ , but the large region of integration of  $E_{np}$  makes the theoretical interpretation difficult. A high resolution experiment not only provides the data at the threshold, but it also provides information about the  $E_{np}$  dependence. In addition, thanks to the high luminosity available at JLab, it will significantly reduce the uncertainties in the  $Q^2$  region that overlaps the existing data.

## 2 Measurements and Theories

Since the original Saclay set of data, two additional experiments have been completed. The first one was the NE4 experiment performed at SLAC which measured the elastic cross section up to  $Q^2 = 70 \text{ fm}^{-2}$  and only as a by-product provided data on the threshold disintegration process [8]. The experiment was optimized to measure the magnetic form factor of the deuteron. The price paid was poor resolution in the scattered electron energy  $E'$ , which led to poor resolution in  $E_{np}$  (as much as 20 MeV FWHM). The poor resolution was a result of spectrometer design and the  $180^\circ$  scattering angle. The extreme backward scattering angle complicated corrections for energy loss in the target and required large radiative corrections (1.2-1.8, depending on choice of model and  $E_{np}$ ). Resolution unfolding, which is manifestly model dependent, was performed to extract cross sections averaged over  $E_{np} = 0 - 10 \text{ MeV}$ .

The second experiment consisted of a set of high resolution measurements performed at Bates [9]. These measurements extend to only  $Q^2 = 42 \text{ fm}^{-2}$ . The authors compared the cross section averaged over  $E_{np} = 0 - 3 \text{ MeV}$  and  $E_{np} = 0 - 10 \text{ MeV}$  and found that the cross section for  $E_{np} = 0 - 10 \text{ MeV}$  varied by -12% to +27% compared to the ones averaged over  $E_{np} = 0 - 3 \text{ MeV}$ . One consistent conclusion drawn from both the SLAC and the Bates data is that the slope of the cross section decreases around  $Q^2 \approx 25 \text{ fm}^{-2}$ . The world's data is shown in Fig. 3.

The dominating systematic error in both the SLAC and the Bates experiment is related to the uncertainty in  $E_{np}$ . For the SLAC experiment, the  $\pm 0.25\%$  uncertainty in the reconstructed energy translated into a  $\pm 20\%$  uncertainty in the resolution unfolded cross section. The Bates experiment suffered from a combination of a 1% beam energy uncertainty, low count rates, and inadequate hydrogen elastic measurements. These deficiencies lead to systematic uncertainties as high as 30%. The measurement discussed in this proposal will not suffer from any of these difficulties, and we expect the error to be dominated by the statistics.

There have been many theoretical investigations of this subject. The initial calculations

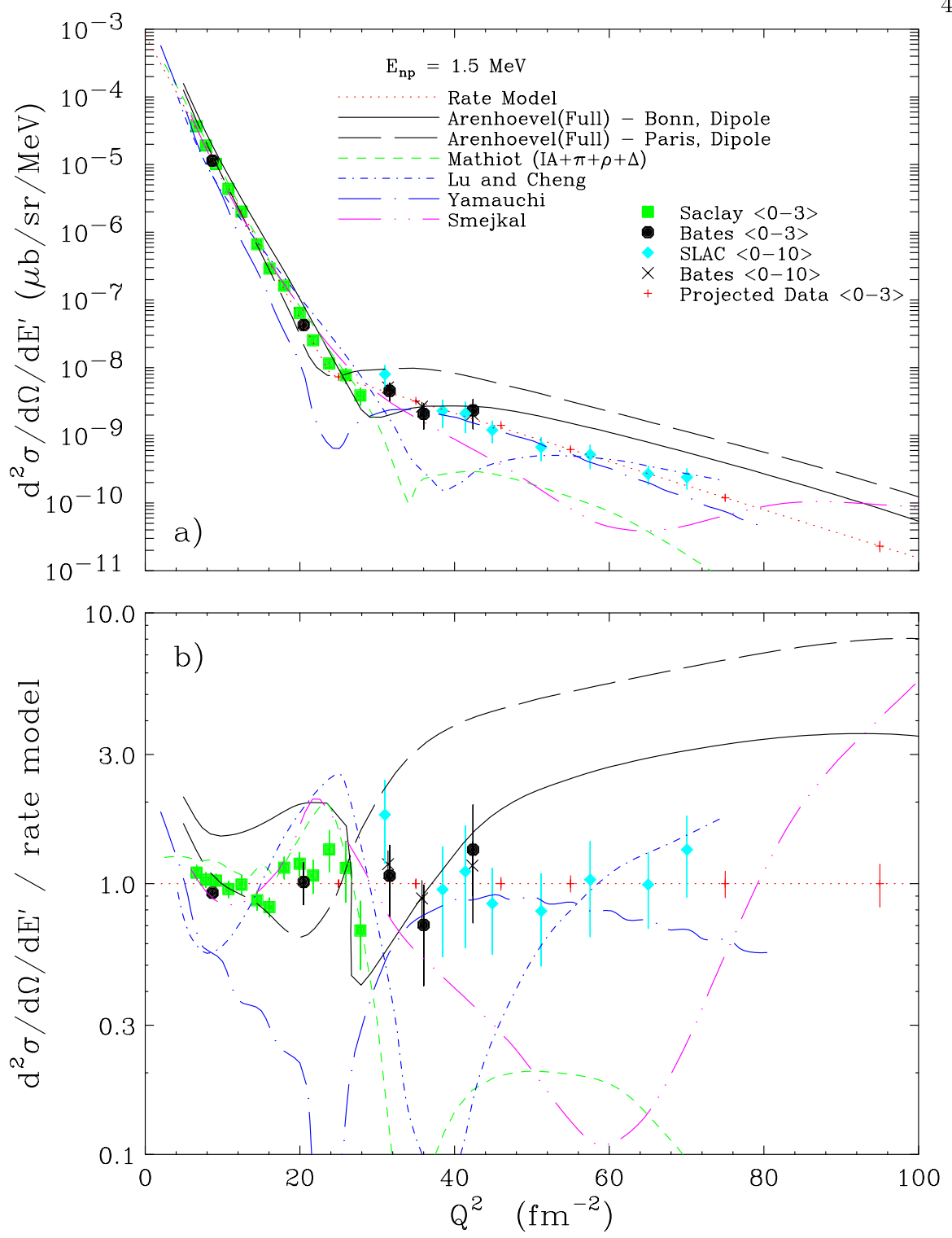


Figure 3: Comparison of several calculations, the world's data and the projected uncertainties for the proposed experiment. The absolute cross section is shown in a) and the cross section relative to the rate model defined in Section 5 is shown in b).

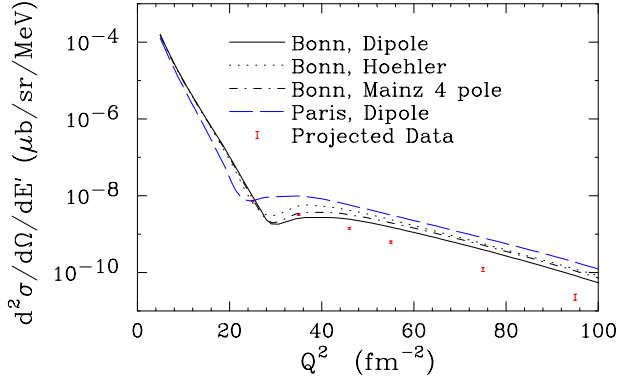


Figure 4: Comparison of calculations from Arenhövel which include MEC+IC+RC. The projected error bars are also shown.

of Mathiot [2], which agreed well with the data for the lower  $Q^2$ , are very sensitive to the monopole cut-off mass  $\Lambda_\pi$  of the  $\pi NN$  vertex. Riska [10] and Buchmann *et al.* [11] avoided this problem by consistently deriving the exchange operators directly from the NN potential. In this approach, the  $\pi NN$  and  $\rho NN$  cut-off masses are implicitly included from the fit of the NN potential parameters to nucleon-nucleon scattering data. Singh *et al.* [12] demonstrated, however, that this approach is sensitive to the choice of NN potential and the parameterization of the nucleon form factors.

A demonstration of the sensitivity to the choice of NN potential and nucleon form factor parameterization is shown in Fig. 4. In the figure, recent calculations from Arenhövel [13] are shown for the Bonn and Paris potentials with the dipole parameterizations, as well as for the Bonn potential with the Höhler [14] and the Mainz 4-pole (Simon) [15] parameterizations. There is a larger variation in the model due to the choice of NN potential than due to form factor parameterization.

All of the baryon configuration space models have a significant dependence on the parameterization of the electromagnetic nucleon form factors. This dependence is misleading. The form factor parameterizations that were explored represent a wide range of authors and experimental databases. No results from the recent high precision form factor measurements have been incorporated into the examined parameterizations. The great wealth of additional form factor results from recent and soon-to-run experiments will greatly restrict the parameterizations and, thus, sharply reduce the cross section model dependence on the form factor parameterization.

In addition to the NN potential dependence, it was initially argued that there was a dependence on the choice of nucleon isovector form factor, either  $G_E^V$  or  $F_1^V$ . The ambiguity in the nucleon form factor arises from the lack of a consistent dynamical theory which describes interacting particles with internal structure. As a result, different approximations are made which lead to different choices of the form factor. Earlier, it was shown that these different form factors lead to different cross sections for deuteron electrodisintegration at threshold [12].

More recently, however, it has been demonstrated that consistent relativistic corrections bring the cross sections for the different form factors into agreement for  $Q^2 \leq 30 \text{ fm}^{-2}$  [16, 17]. Above this  $Q^2$ , differences in the cross section are simply an indication of inadequate relativistic corrections.

One fundamental question of nuclear physics is: At what point does the mesonic and nucleonic description of the NN interaction begin to break down and nucleonic substructure and dynamics begin to become important? Deuteron electrodisintegration at threshold at high momentum transfers, a process in which non-nucleonic contributions are important, is an ideal means to study this issue.

Several attempts have been made to simultaneously describe the quark- and gluon-exchange mechanism at short distance and the meson-exchange mechanism at long and intermediate distance in the electrodisintegration of the deuteron. One such hybrid model, developed by Cheng and Kisslinger [18], divided the deuteron into two distinct regions: an exterior one, described by baryon configurations, and an interior one, described by six quark (6q) configurations. When the internucleon separation is smaller than the matching radius  $r_0 \approx 1 \text{ fm}$  of the two regions, the deuteron is treated as a 6q configuration with a certain probability given by the overlap integral of the 6q wave function inside the matching radius. Their model predicted a second maximum in the cross section at  $Q^2 \approx 50 \text{ fm}^{-2}$ , which they described as a signature of the 6q clusters. This bump, however, is not seen in either the Bates or the SLAC data. Glozman *et al.* [19] treated the deuteron in a similar way, but without the artificial separation of the nucleonic and 6q configuration spaces.

A recent extension of the Cheng and Kisslinger model was performed by Lu and Cheng [20]. They added isoscalar MEC to the model, however contributions from this mechanism affected the longitudinal part of the cross section and left the transverse part almost unchanged. Lu and Cheng demonstrated that as  $E_{np}$  increases the maximum that is characteristic of the 6q cluster gets smaller and eventually disappears altogether by  $E_{np} = 10 \text{ MeV}$ . They conclude that the SLAC experiment would not observe the signature 6q bump and that “further experiments with good resolution in the range of small  $E_{np}$  would be highly desirable.”

There is another interesting observation about the Lu and Cheng model. The signature 6q bump disappears for model calculations which exclude either the isovector MEC or the 6q cluster contributions. This result implies that the bump is due to an interference between these two contributions. Therefore, alterations in either of these contributions could change the character of the signature of the 6q bump.

Another possible means to alter the character of the 6q bump is to change the matching radius  $r_0$ . Cheng and Kisslinger used  $r_0 = 1.0 \text{ fm}$  while Lu and Cheng used  $r_0 = 0.8 \text{ fm}$ . This small change in  $r_0$  shifts the minimum in the cross section from  $Q^2 = 28 \text{ fm}^{-2}$  to  $Q^2 = 36 \text{ fm}^{-2}$ .

It is conceivable, therefore, that a small shift in  $r_0$  and/or changes in the MEC current or 6q cluster contributions could significantly modify the prediction of the signature 6q bump so that it appears at a higher  $Q^2$  than was measured by the Bates experiment.

A quark-based approach more ambitious than the hybrid model is the resonating group method (RGM) as followed by Yamauchi *et al.* [21] and Chemtob and Furui [22]. In RGM, the two-baryon system is described as a composite of six equivalent quarks whose states are represented in terms of a three quark cluster basis. The interaction mechanisms consist of quark-interchange effects, gluon-exchange perturbative corrections and pion-exchange effects.

The most recent model is a chiral Lagrangian calculation from Smejkal, Truhlík and Göller [23]. They construct their Lagrangian in a  $N\pi\rho a_1$  system<sup>1</sup> in the framework of hidden local symmetries. In this framework, the mass terms of the gauge fields are incorporated via a local group. The exchange currents include  $\pi + \rho$  MEC and  $a_1 - \pi$  exchange currents. They find that the model dependence of their calculation is about one-third of the variation due to different parameterizations of the electromagnetic nucleon form factors, but that the model dependence is at the level of previous experimental errors.

The various models discussed in this proposal and the world's data for deuteron electrodisintegration is shown in Fig. 3. While most of the models agree with some of the data, none of them agree with all of the data, particularly in the high  $Q^2$  region. The predicted errors for the proposed measurements are also shown. Clearly, this experiment will be able to differentiate between the various models and bring us closer to a better understanding of the short-range part of the NN interaction.

#### *An Illustrative Example:*

There are many qualitative things one can learn from a closer examination of the results from recent calculations of Arenhövel. It should be noted that because of the order of the relativistic corrections (RC), these calculations are quantitatively reliable up to  $Q^2 \approx 30 \text{ fm}^{-2}$ . Above this  $Q^2$ , the calculations should be viewed as qualitative only.

The cross section with different contributions are shown in Fig. 5. At higher  $Q^2$ , MEC continue to play a significant role while IC are not so important. RC significantly enhance the cross section for  $Q^2 > 45 \text{ fm}^{-2}$ .

A comparison between the PWBA+RC and the NORMAL+RC calculation provides some qualitative information about the importance of the nearly bound  $^1S_0$  state in the final state. In the PWBA+RC calculation, the final state is forced to be in plane waves, whereas the effect

---

<sup>1</sup>The  $\rho$  and  $a_1$  (formerly known as  $A_1$ ) are the gauge particles of the groups  $[\text{SU}(2)_L \times \text{SU}(2)_R]_{\text{global}}$  and  $[\text{SU}(2)_L \times \text{SU}(2)_R]_{\text{local}}$  [24, 25].

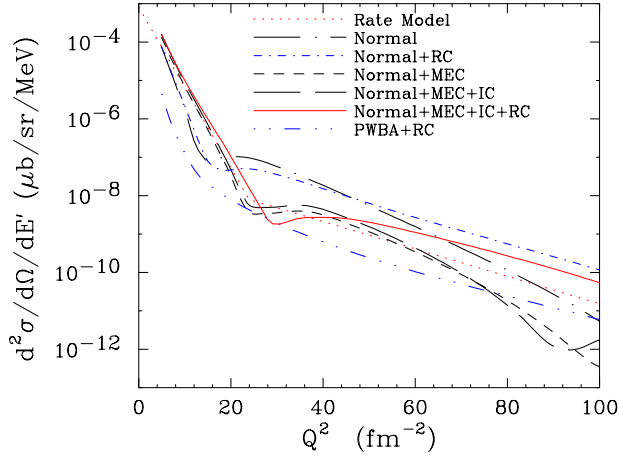


Figure 5: Recent calculations with various contributions from Arenhövel. The calculations were performed with the Bonn potential and the dipole form factor fit and were averaged over  $E_{np} = 0 - 3$  MeV.

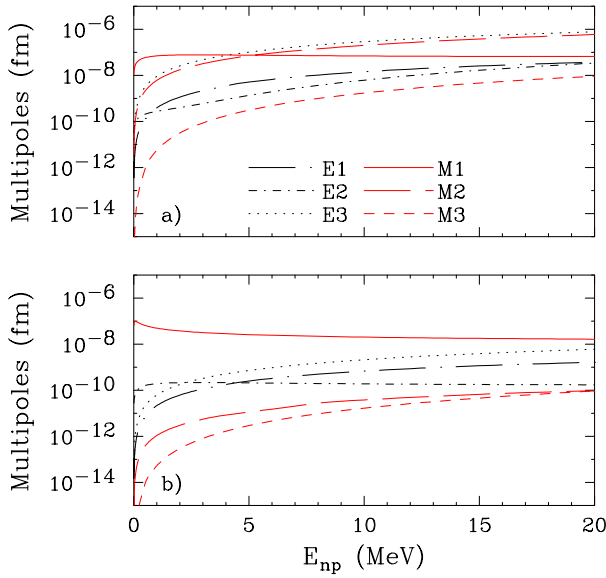


Figure 6: Comparison of  $E_{np}$  dependence of multipoles from recent Arenhövel calculations for  $Q^2 =$  a)  $27.9 \text{ fm}^{-2}$  and b)  $81.7 \text{ fm}^{-2}$ . The upper plot is near the minimum of the full calculation, and the lower plot reflects the typical dominance of the  $M1$  over the other multipoles for  $Q^2$  not near the minimum.

of the  $^1S_0$  state on the final state is included in the NORMAL calculations. The NORMAL calculation is an order of magnitude larger than the PWBA calculation for  $Q^2 > 20 \text{ fm}^{-2}$ . This difference does not vary strongly with  $Q^2$ , because the effect of the final state interactions is determined by the relative energy of the n-p final state, which is held fixed by examining  $E_{np} = 0 - 3$  MeV. Thus the  $^1S_0$  state has a profound effect on the final state, signaling the sensitivity of deuteron electrodisintegration at threshold to the IV M1 transition.

The leading transverse multipoles as a function of  $E_{np}$  for two  $Q^2$ 's, one near and one far from the interference minimum, are shown in Fig. 6. At the interference minimum, the  $M1$  amplitude no longer dominates for  $E_{np} > 5$  MeV. Away from the minimum, the  $M1$  remains an order of magnitude larger than all other multipoles up to  $E_{np} \approx 10$  MeV. This result emphasizes the importance of a high resolution measurement.

The variation in  $E_{np}$  for different  $Q^2$  is shown in Fig. 7. In this figure, the cross section as

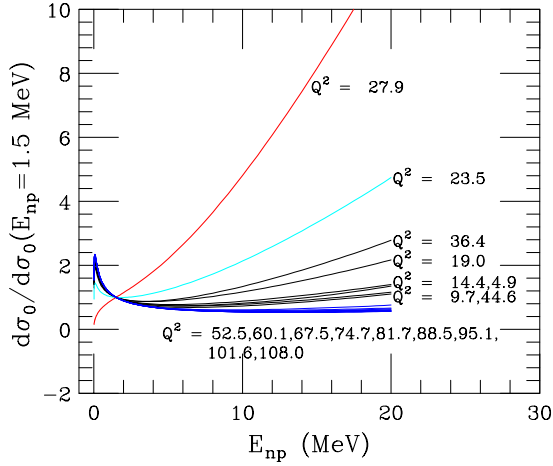


Figure 7: Relative cross sections as a function of  $E_{np}$  for various  $Q^2$  from recent Arenhövel calculations. The listed  $Q^2$  are in  $\text{fm}^{-2}$ .

a function of  $E_{np}$  is drawn for a selection of  $Q^2$ . The curves have been normalized to unity at  $E_{np} = 1.5$  MeV. There is a very strong variation depending on the proximity to the interference minimum of the cross section. If, for example, that minimum were to shift by  $4 \text{ fm}^{-2}$ , there would be a considerable change in the dependence on  $E_{np}$ . This observation reemphasizes the importance of a high resolution measurement.

Finally, we demonstrate the effect of averaging over different ranges of  $E_{np}$  in Fig. 8. The minimum in the cross section is washed out for the  $E_{np} = \langle 0 - 10 \rangle$  MeV range, however the slope of the cross section versus  $Q^2$  is not affected. The results shown in Fig. 8 vary little with the choice of NN potential or nucleon form factor. Again, we stress that these results are only qualitative.

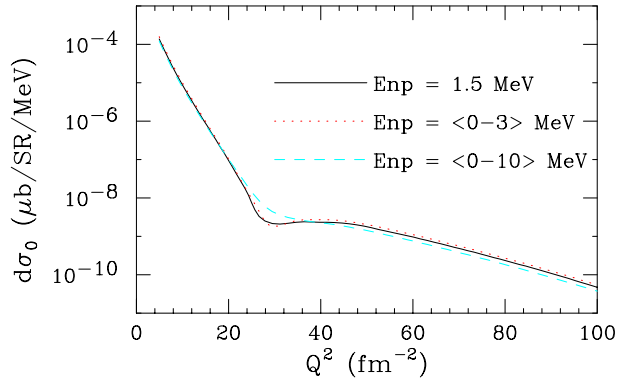


Figure 8: Effect of averaging the cross section over different ranges in  $E_{np}$  for the recent Arenhövel calculations. There is little dependence on the choice of NN potential and form factor fits.

### 3 Experimental Setup

This experiment will measure transverse deuteron electrodisintegration at threshold which is sensitive to the isovector magnetic dipole part of the NN interaction. At the chosen kinematics,

	$Q^2$ ( $\text{fm}^{-2}$ )	$Q^2$ (( $\text{GeV}/c$ ) $^2$ )	$E$ ( $\text{GeV}$ )	$E'$ ( $\text{GeV}$ )	$\partial E_{np}/\partial E$	$\partial E_{np}/\partial E'$	$\partial E_{np}/\partial \theta_e$ ( $\text{MeV}/\text{mrad}$ )
	25	0.97	0.65	0.39	0.599	1.668	0.046
	35	1.36	0.80	0.44	0.547	1.828	0.064
	45	1.75	0.95	0.48	0.506	1.976	0.082
	55	2.14	1.08	0.51	0.472	2.117	0.100
	75	2.92	1.34	0.56	0.419	2.384	0.137
	95	3.70	1.59	0.60	0.379	2.639	0.174

Table 1: List of proposed kinematics and the derivatives related to the resolution in  $E_{np}$ . The three partial derivatives define the contribution of the beam energy  $E$ , the scattered electron energy  $E'$ , and the scattering angle  $\theta_e$  to the excitation energy resolution.

non-baryon degrees of freedom should play a significant role. For this measurement, it is necessary to perform a high resolution, high luminosity, single-arm experiment at backward angles with low background rates.

The scattering angle is fixed at the most backward angle of the HRS<sub>e</sub>,  $160^\circ$ , to minimize contributions from the elastic cross section and the longitudinal part of the disintegration cross section. The luminosity is maximized by using 120  $\mu\text{A}$  beam on a 2 cm wide 15 cm long cell. The luminosity is limited by the end station refrigerator, assuming the other halls are not placing significant cryogenic demands.

The choice of  $Q^2$  reflects several constraints. The minimum  $Q^2$  was chosen to correspond to the point at which the cross section appears to change slopes. The maximum  $Q^2$  is limited by the expected cross section of  $9 \cdot 10^{-42} \text{ cm}^2/\text{sr MeV}$ . The density of measurements up to  $Q^2 = 55 \text{ fm}^{-2}$  reflects the possible structure of the cross section that most models predict in this region, see Fig. 3. Finally, to keep the number of measurements to a minimum, and hence the number of beam energy changes, only one  $Q^2$  between 55 and  $95 \text{ fm}^{-2}$  was chosen. This selection of  $Q^2$  offers some overlap with previous measurements and significantly extends the range of  $Q^2$ . We are flexible with beam energy for an individual measurement to roughly  $\pm 30 \text{ MeV}$ . A list of the proposed kinematics is shown in Table 1.

The high resolution is important for a few reasons. For the low  $Q^2$  points, it is necessary to separate the elastic peak from the disintegration data. For all  $Q^2$  points, the higher resolution in  $E_{np}$  will provide information on the  $E_{np}$  dependence in addition to the  $Q^2$  dependence. As discussed earlier, the high resolution is vital in establishing a clear theoretical interpretation. Finally, the high resolution minimizes systematic uncertainties involved in the resolution un-

folding process, such as those from which the SLAC data suffered. As will be discussed in the following section, the resolution is limited by the target design and the HRS exit window but not by the resolutions of the HRS.

Three modifications to the standard setup should be done to enhance the resolution and performance.

- The vacuum system of the HRS<sub>e</sub> should be directly attached to the target chamber, thus eliminating the target chamber window and spectrometer entrance window.
- The use of a 2 cm wide target cell, like the high pressure helium cell already planned for Hall A [26]. The narrow cell would minimize the material along the tracks. This is important as straggling in the deuterium of the scattered electron is the dominate contributor to the  $E_{np}$  resolution if we were to use the current LH<sub>2</sub>/LD<sub>2</sub> cells. We require two such cells: one for LD<sub>2</sub> and one for LH<sub>2</sub>.
- A fixed collimator will be placed next to the target cell to minimize contributions from the target endcaps. This collimation is critical as the quasielastic cross section will be large compared to the deuteron cross section.

It is important to minimize and understand the background online. At the highest  $Q^2$ , the count rate is  $\approx 3$  counts per day. It will be necessary to require for the trigger either a coincidence among the Čerenkov counter, the hodoscope, and a minimal shower signal or a coincidence between the hodoscope and a large shower signal.

Offline elimination of background is also important. The tight correlation of the position and angular divergence of the scattered electrons in the drift chambers will restrict the possible particles to be electrons and pions coming from the target and a small fraction of the cosmic background. The Gas Čerenkov counter will eliminate the pions coming from the target and low energy cosmics. The lead-glass shower counters will greatly reduce high energy cosmics. This scheme has already been well established in both the Bates and the SLAC experiments.

## 4 $E_{np}$ Resolution

The resolution in the relative separation energy of the final  $np$  system  $\Delta E_{np}$  is a function of the scattering angle  $\theta$ , the beam energy  $E$  and the scattered electron energy  $E'$  and their associated experimental uncertainties  $\Delta\theta$ ,  $\Delta E$  and  $\Delta E'$ :

$$\Delta E_{np} = \sqrt{\left(\frac{\partial E_{np}}{\partial E} \Delta E\right)^2 + \left(\frac{\partial E_{np}}{\partial E'} \Delta E'\right)^2 + \left(\frac{\partial E_{np}}{\partial \theta} \Delta \theta\right)^2}, \quad (1)$$

where

$$\frac{\partial E_{np}}{\partial E} = \frac{M - 2E' \sin^2(\theta/2)}{W} \approx \frac{E'}{E}, \quad (2)$$

$$\frac{\partial E_{np}}{\partial E'} = \frac{M + 2E' \sin^2(\theta/2)}{W} \approx \frac{E}{E'}, \quad (3)$$

$$\frac{\partial E_{np}}{\partial \theta} = \frac{EE' \sin \theta}{W} \approx \frac{EE' \sin \theta}{M_d}. \quad (4)$$

The three partial derivatives which define the contributions of the  $\Delta\theta$ ,  $\Delta E$  and  $\Delta E'$  uncertainties are given together with the proposed kinematic settings in Table 1.

The expected FWHM uncertainties in the incident and scattered electron energies and in the scattering angle as calculated using analytic formulas are given in Table 2 for the extreme kinematics. The calculations assume

- a 2.0 cm wide cell that is 15 cm long surrounded by 13 mil aluminum walls and entrance window,
- a scattering angle of  $160^\circ$ ,
- 4 mil Ti exit window in the HRS,
- momentum resolution of  $1 \cdot 10^{-4}$ ,
- a transverse position resolution of 0.15 cm, or 0.44 cm along the beam,
- scattering angle resolution of 1 mrad,
- multiple scattering due to the 4 mil Ti exit window is 1.1 mrad at  $\delta = 2.25\%$  for 1 GeV central momentum.

The beam energy uncertainty  $\Delta E$  is dominated by straggling in the deuterium. Straggling in the target entrance window is a minor effect. The excellent transverse position resolution  $\Delta y_0$  of the HRS in the non-bend plane will allow reconstruction of the origin  $z_0$  of the events in the target. This information will be used to correct for the probable energy loss of the incident electrons. The resolution of the vertex reconstruction is a much smaller effect than the straggling in the deuterium.

The scattered energy uncertainty  $\Delta E'$  is dominated by straggling in the deuterium. Straggling in the cell wall and spectrometer resolution play only a minor role.

The scattering angle uncertainty  $\Delta\theta$  is due to multiple scattering of the incident and scattered electron in the liquid deuterium, the target entrance endcap and exit wall and the exit window of the HRS. The dominate contributions are from multiple scattering in the cell walls

	$Q^2(\text{fm}^{-2})$	
	25	95
$\Delta E$ (MeV)		
Straggling in LD <sub>2</sub>	0.69	0.69
Straggling in Al	0.05	0.05
Probable energy loss	0.13	0.14
TOTAL	0.71	0.71
$\Delta E'$ (MeV)		
Straggling in LD <sub>2</sub>	0.27	0.27
Straggling in Al	0.14	0.14
Spectrometer resolution	0.04	0.06
TOTAL	0.31	0.31
$\Delta\theta$ (mr)		
Multiple scattering in LD <sub>2</sub> ( $e$ )	4.1	1.7
Multiple scattering in Al ( $e$ )	2.3	1.0
Multiple scattering in LD <sub>2</sub> ( $e'$ )	4.2	2.7
Multiple scattering in Al ( $e'$ )	7.2	4.6
Spectrometer resolution	1.0	1.0
Exit window	6.7	4.3
TOTAL	11.7	7.2

Table 2: FWHM energy and angular resolutions for the two extreme kinematics.

and the exit window. The contributions of the exit window are taken from Ref. [27]. In this reference the angular resolution is given for 1 GeV and 4 GeV electrons. Assuming that the resolution is determined by multiple scattering, we scaled the result for 1 GeV electrons at  $\delta = 2.25\%$  by  $1/E'$  for our kinematics. This assumption probably overestimates the effect at lower energies because it underestimates the 4 GeV results based on the 1 GeV resolutions.

The total FWHM  $\Delta E_{np}$  resolution and its separate components as a function of momentum transfer for  $\theta = 160^\circ$  are given in Table 3. The dominate contributor to the  $E_{np}$  resolution is the multiple scattering in the aluminum walls of the cell and the Ti exit windows, however, there are several almost as large contributions. The HRS angular and momentum resolutions make no sizeable contribution to the overall  $\Delta E_{np}$ . While we would warmly use a thin walled cell or a thinner exit window, the advantages are not significant enough to justify the development for this experiment alone.

$Q^2$ ( $\text{fm}^{-2}$ )	Due to $\Delta E$ (MeV)	Due to $\Delta E'$ (MeV)	Due to $\Delta\theta$ (MeV)	Total $\Delta E_{np}$ (MeV)
25	0.42	0.51	0.54	0.85
35	0.39	0.56	0.65	0.94
45	0.36	0.61	0.76	1.04
55	0.33	0.65	0.87	1.13
75	0.30	0.73	1.06	1.33
95	0.27	0.82	1.25	1.52

Table 3: Contribution of various components to the FWHM  $E_{np}$  resolution for the proposed kinematics

## 5 Rates

The cross section for estimating the rates is based on a fit to the Saclay and SLAC data. Those two data sets are independently fit to an exponential function. At the  $Q^2$  where the two fitted curves meet, the cross section instantly switches from one curve to the other. This ‘‘Rate Model’’ is plotted in Fig. 3 along with the world’s data.

The following quantities were used in the rate estimates:

$$\begin{aligned}
 \text{beam current} &= 120 \mu\text{A} \\
 \theta_e &= 160^\circ \\
 \text{effective target length} &= 10 \text{ cm} \\
 \text{radiative correction} &= 0.7 \\
 \text{solid angle} &= 6.4 \text{ msr} \\
 \Delta E_{np} &= 3 \text{ MeV}
 \end{aligned}$$

After geometrical considerations of a likely target collimator, only 10 of the 15 cm of the target are effectively viewable by the HRS<sub>e</sub>. The resulting luminosity is  $3.6 \cdot 10^{38} \text{ cm}^{-2}\text{s}^{-1}$ . The solid angle considers the extended target acceptance [28]. The estimated rates, along with run times and statistical errors, are shown in Table 4.

The experiment will be calibrated with elastic electron-deuteron scattering for low  $Q^2$  and with elastic electron-proton scattering for all  $Q^2$ . The spectrometer optical properties and solid angle will be checked by comparing the elastic peak distributions in the drift chambers with the predicted ones from a Monte Carlo model of the spectrometer. Both deuteron and proton elastic cross sections and rates are shown in Table 5. The luminosity used to determine the proton elastic rates was  $3.2 \cdot 10^{38} \text{ cm}^{-2}\text{s}^{-1}$ .

$Q^2$ ( $\text{fm}^{-2}$ )	$d\sigma/d\Omega dE_{np}$ ( fb/sr MeV)	Rate (counts/h)	Time (h)	Stat. Error (%)
25.0	4.36	77.1	11	3.4
35.0	1.75	30.9	17	4.3
45.0	0.712	12.6	27	5.5
55.0	0.292	5.17	40	7.0
75.0	0.0501	0.886	90	11.2
95.0	0.00876	0.155	199	18.0

Total Time: 384

Table 4: Estimated rates and possible run plan. The rates have been estimated using the fit to the Saclay and SLAC data as described in the text.

Deuteron Elastics				Proton Elastics		
$Q^2$ ( $\text{fm}^{-2}$ )	$d\sigma/d\Omega$ (fb/sr)	Rate (counts/h)	Stat. Error (%)	$Q^2$ ( $\text{fm}^{-2}$ )	$d\sigma/d\Omega$ (fb/sr)	Rate (counts/s)
25	67.3	397	1.5	17.9	$1.13 \cdot 10^6$	1614
35	6.27	37.0	4.0	24.2	$4.74 \cdot 10^5$	678
45	0.867	5.11	8.5	30.2	$2.29 \cdot 10^5$	328
55	0.258	1.52	12.8	36.1	$1.22 \cdot 10^5$	175
75				47.6	$4.23 \cdot 10^4$	60.5
95				58.7	$1.75 \cdot 10^4$	25.0

Table 5: Proton and deuteron elastic cross sections and rates. For the deuteron elastics, the kinematics are identical to those of the deuteron disintegration measurement. For  $Q^2 > 60 \text{ fm}^{-2}$ , the deuteron elastic kinematic are beyond the range of the database used to fit the  $Q^2$  dependence of the cross section. For the proton elastics, the beam energy and scattering angle from the corresponding deuteron measurement were used to determine  $Q^2$ . Note that the proton rates are in counts per second while the deuteron rates are in counts per hour.

Item	Time (hours)
setup	72
check out	48
physics measurements	384
empty target measurements	38
hydrogen elastic measurements	6
decommissioning	24
total beam time	476
total time	572

Table 6: Time budget

A summary of the time budget can be found in Table 6. The installation of the experiment will be relatively straight forward with the installation of the target collimator and the target chamber window that attaches directly to HRS<sub>e</sub>. The check-out time is for diagnostics of the system with beam. There is essentially no overhead for the empty target and hydrogen elastic measurements. We assume that the small width cryotarget is already installed, and we do not include any time for beam energy changes. The total beam time request is 476 hours or 20 days.

## 6 Commitment of the Collaborators

All collaborators will participate in the actual setup and data taking for the experiment. The University of Basel group intends to participate in the design and construction of the target chamber window that connects directly to the HRS<sub>e</sub> as well as the target collimator. Once the experiment is approved, the proposal authors will seek to include the Hall A collaboration as participants.

## 7 Summary

We propose to perform a high resolution measurement of the transverse deuteron electrodisintegration at threshold for large momentum transfers. Near threshold, the theoretical description of the reaction simplifies so that an isovector magnetic dipole transition is dominant. At lower  $Q^2$ , this reaction is proven to be sensitive to non-nucleonic contributions of the nucleon-nucleon interaction, such as MEC. At higher  $Q^2$ , it should be sensitive to the quark and gluonic de-

degrees of freedom. This measurement will significantly extend the  $Q^2$  of previous data, provide significantly reduced errors, and provide reliable  $E_{np}$  and  $Q^2$  dependence. There already exists considerable theoretical interest in this study [29], and more precise data will only enhance that interest. We expect the results of this experiment to challenge the simple non-relativistic picture of the deuteron and enhance our understanding of the two nucleon system.

The maximum  $Q^2$  is limited by the smallest possible count rate, which we expect to correspond to cross sections of the order of  $9 \cdot 10^{-42}$  cm<sup>2</sup>/sr MeV. This measurement requires mostly standard Hall A equipment: the HRS<sub>e</sub> and associated electronics and the planned high pressure helium target cells, albeit with liquid deuterium and hydrogen. In addition, we need a collimator to shield the target walls and a means to attach the HRS<sub>e</sub> directly to the target vacuum chamber. The measurement can be completed in 20 days of beam time and 4 days for setup and decommissioning.

## References

- [1] M. Bernheim *et al.*, Phys. Rev. Lett. **46**, 402 (1981). S. Auffret *et al.*, Phys. Rev. Lett. **55**, 1362 (1985).
- [2] J.F. Mathiot, Nucl. Phys. **A412**, 201 (1984).
- [3] R.B. Wiringa, R.A. Smith and T.A. Ainsworth, Phys. Rev. C **29**, 1207 (1984).
- [4] R. Machleidt, K. Holinde, Ch. Elster, Phys. Rep. **149**, 1 (1987).
- [5] M. Lacombe *et al.*, Phys. Rev. C **21**, 861 (1980). M. Lacombe *et al.*, Phys. Lett. **B101**, 139 (1981).
- [6] M.M. Nagels, T.A. Rijken and J. de Swaart, Phys. Rev. D **17**, 769 (1978).
- [7] [http://www.jlab.org/exp\\_prog/PACpage/PAC14/FewBodyWkshp.ps](http://www.jlab.org/exp_prog/PACpage/PAC14/FewBodyWkshp.ps)
- [8] M. Frodyma *et al.*, Phys. Rev. C **47**, 1599 (1993). R.G. Arnold *et al.*, Phys Rev C **42**, R1 (1990).
- [9] W.M. Schmitt *et al.*, Phys. Rev. C **56**, 1687 (1997). K.S. Lee *et al.*, Phys. Rev. Lett. **67**, 2634 (1991).
- [10] D.O. Riska, Phys. Scr. **31**, 107 (1985).
- [11] A. Buchmann, W. Leidemann, H. Arenhövel, Nucl. Phys. **A393**, 385 (1983).

- [12] S. K. Singh, W. Leidemann, H. Arenhövel, *Z. Phys. A* **331**, 509 (1988).
- [13] H. Arenhövel, private communication (2000).
- [14] G. Höhler *et al.*, *Nucl. Phys.* **B114**, 505 (1976).
- [15] G.G. Simon *et al.*, *Nucl. Phys.* **A333**, 381 (1979).
- [16] T. Wilbois, G. Beck, H. Arenhövel, *Few Body Sys* **15**, 39 (1993).
- [17] G. Beck, T. Wilbois, H. Arenhövel, *Few Body Sys* **17**, 91 (1994).
- [18] T.S. Cheng and L.S. Kisslinger, *Nucl. Phys.* **A457**, 602 (1986).
- [19] L.Y. Glozman *et al.*, *Phys. Lett. B* **200**, 406 (1988).
- [20] L.C. Lu and T.S. Cheng, *Phys. Lett. B* **386**, 69 (1996).
- [21] Y. Yamauchi *et al.*, *Phys. Lett. B* **146**, 153 (1984).
- [22] M. Chemtob and S. Furui, *Nucl. Phys.* **A449**, 683 (1986).
- [23] J. Smejkal, E. Truhlík, H. Göller, *Nucl. Phys.* **A624**, 655 (1997).
- [24] M. Bando, T. Kugo, K. Yamawaki, *Phys. Rep.* **164**, 217 (1988).
- [25] U.-G. Meißner, *Phys. Rep.* **161**, 213 (1988).
- [26] J.-P. Chen, private communication (2000).
- [27] J. LeRose, Jefferson Lab TN-00-001 (2000).
- [28] G.G. Petratos, private communication (2000).
- [29] For example, F. Gross and G. Gerstner are currently performing new calculations and D. Phillips has expressed interest in performing calculations in the future.